

# Effect of Solution-Treatment on Microstructure and Mechanical Properties of Cast Fine-Grain CM 247 LC Superalloy

Hsin-Erh Huang\*<sup>1</sup> and Chun-Hao Koo\*<sup>2</sup>

Department of Materials Science and Engineering, National Taiwan University, Taipei, 106 Taiwan, R. O. China

This study investigates the effect of the solution-treatment, with solution temperatures from 1494 to 1533 K, on the microstructure and mechanical properties of fine-grain (65  $\mu\text{m}$ ) CM 247 LC superalloy. Tensile tests reveal that the yield strength of the alloy after multi-step 1527 K/2 h solution-treatment exceeds that after 1494 K/2 h solution-treatment. Additionally, the alloy after multi-step 1527 K/2 h solution-treatment had a lower creep rate and greater rupture life than that after 1494 K/2 h solution-treatment. The improved mechanical properties are attributed to the high volume fraction of  $\gamma'$  particles with the proper size and the refinement of carbides, which inhibit the gliding and climbing of dislocations.

(Received October 30, 2003; Accepted February 20, 2004)

**Keywords:** Cannon-Muskegon 247 Low-Carbon Superalloy,  $\gamma'$  particle, carbide, mechanical properties, solution-treatment

## 1. Introduction

Integrally cast turbine wheels have been extensively used in turboprop and auxiliary power gas turbine engines for several years.<sup>1)</sup> The operating temperature of the turbine disk generally does not exceed 1033 K. Operating stresses due to the centrifugal loads of these rotating components usually exceed 550 MPa at the rim and toward the center. However, turbine blades are subjected to relatively low stress, typically below 345 MPa, but high operating temperature. Materials applied in the wheel must combine the properties of the blade and the disk. Generally, a microstructure with numerous and randomly orientated equiaxed grains is necessary to yield favorable mechanical properties. However, establishing such a microstructure in thin sections is difficult. To achieve this objective, however, the Microcast-X casting process, developed by Howmet Turbine Components Corporation, has been successfully demonstrated to form components from turbine disks to blades and vanes. Integrally cast fine grain turbine wheels have been extensively cast using IN 713 LC, IN 718, and Mar-M247 nickel-based superalloys.<sup>1-5)</sup> The strict requirements of the high operating temperatures of integral turbine wheels, the increased rotational speeds and the extended lifetimes of components have forced designers of turbine engines to tighten their criteria for selecting alloys.

The CM 247 LC superalloy is a cast nickel-based superalloy with low carbon content.<sup>6-8)</sup> The alloy is a modified superalloy based on the chemical composition of

Mar-M247, specifically designed for fabricating directionally solidified (DS) turbine blades. The authors' previous study<sup>9)</sup> indicated that, when the casting parameters are well-controlled, the CM 247 LC superalloy has an excellent castability that can be exploited form an equiaxed grain structure, with high strength and superior creep resistance. However, the effect of heat treatment on the tensile strength and creep performance of the fine grain CM 247 LC superalloy is still controversial.

The Microcast-X casting process was used herein to produce test specimens of a CM 247 LC superalloy with a controlled fine-grain structure. The objective of this work is to investigate the microstructure and tensile and creep performance of the fine-grain CM 247 LC superalloy after solution-treatment at various temperatures. Moreover, some mechanisms associated with microstructural changes and improved mechanical properties are discussed.

## 2. Experimental Procedure

The alloys used herein were originally melted by vacuum induction melting (VIM) at the Cannon-Muskegon Corporation in USA. The alloys were remelted in an alumina crucible in a VIM furnace and poured at 1643 K into a ceramic shell mold with a CoO facecoat, at the Chung Shan Institute of Science and Technology in Taiwan. The ceramic shell mold was maintained at 1373 K. Table 1 presents the nominal composition of the as-cast alloy, which meets the

Table 1 Nominal composition (mass%).

Alloys	C	Cr	Co	W	Mo	Ta	Al	Ti	Hf	B	Zr	Ni
EMS-73687 Spec.	0.07–0.08	8.0–8.5	9.0–9.5	9.3–9.7	0.5–0.6	3.1–3.3	5.4–5.7	0.6–0.9	1.2–1.6	0.01–0.02	0.007–0.015	BAL
CM 247 LC As-cast	0.075	8.1	9.2	9.5	0.5	3.2	5.6	0.7	1.4	0.015	0.015	BAL

\*<sup>1</sup>Graduate Student, National Taiwan University

\*<sup>2</sup>Corresponding author, E-mail: chkoo@ccms.ntu.edu.tw

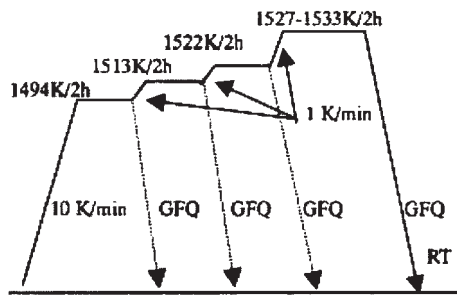


Fig. 1 The processes of solution-treatment in this research. GFQ represents gas fan quenching.

Honeywell EMS-73687 aerospace engineering material specification. After all cast test bars underwent hot isostatic pressing (HIP) at 1458 K/173 MPa/4 h in an atmosphere of argon, they were heat-treated in a vacuum. The heat treatment schedules consisted of multi-step solution-treatments from 1494 K/2 h to 1533 K/2 h, followed by argon gas fan quenching (Ar-GFQ), as depicted schematically in Fig. 1. Finally, the test bars were subject to double aging treatments at 1353 K/4 h and 1144 K/20 h, with Ar-GFQ in each stage. The just size of the test bars was 6.3 mm in diameter by 25.4 mm long. The microstructure was elucidated by optical microscopy (OM) and scanning electron microscopy (SEM). The grain size and the area fraction of the  $\gamma$ - $\gamma'$  eutectic nodules were measured using the linear intercept method. The morphology of  $\gamma'$  particle and MC carbide were also examined. Tensile tests were carried out at room temperature using an Instron 1125 mechanical testing machine at a strain rate of  $8.3 \times 10^{-4} \text{ s}^{-1}$ . The creep and rupture tests were conducted in air at 1255 K with applied stresses of 104, 200 and 345 MPa, using SATEC M3 creep testers.

### 3. Results

#### 3.1 Microstructure and characteristics of carbides

Figure 2 depicts the typical as-cast microstructure of the fine-grain CM 247 LC superalloy. The structure comprises

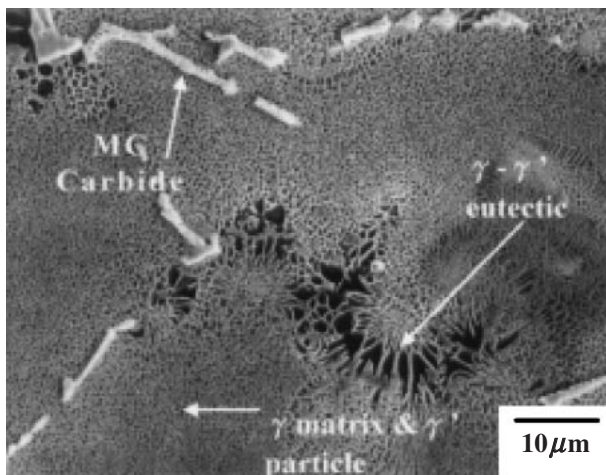


Fig. 2 SEM micrograph showing the as-cast microstructure of fine grain CM 247 LC superalloy.

$\gamma$ - $\gamma'$  eutectic phases,  $\gamma'$  particles and MC carbides. The primary  $\gamma$ - $\gamma'$  eutectic phase is present mainly at the grain boundaries, with a small portion within the grains. The as-cast MC carbide has a predominantly script-like shape. The average grain size of approximately  $65 \mu\text{m}$ , as shown in Fig. 3, was obtained by maintaining the pouring temperature

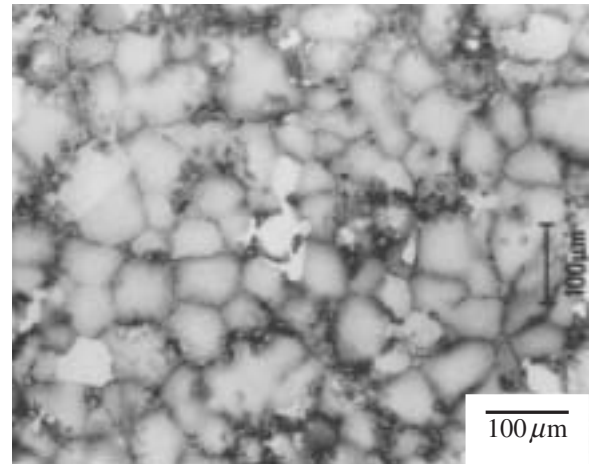


Fig. 3 Optical micrograph showing the grain size of fine grain CM 247 LC superalloy. The average grain size is  $65 \mu\text{m}$ .

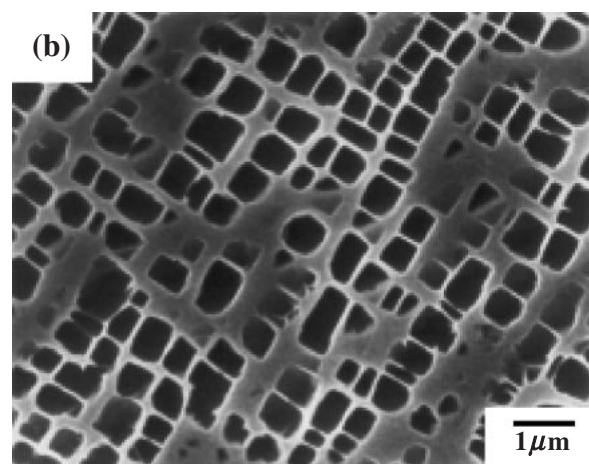
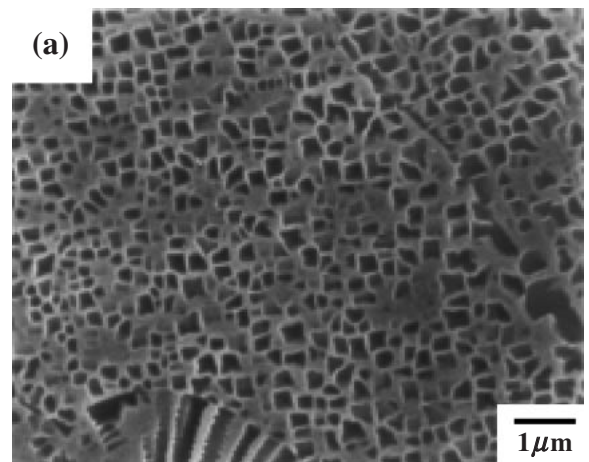


Fig. 4 SEM micrographs showing the morphology of  $\gamma'$  particles in fine grain CM 247 LC superalloy: (a) as-cast, (b) after HIPing.

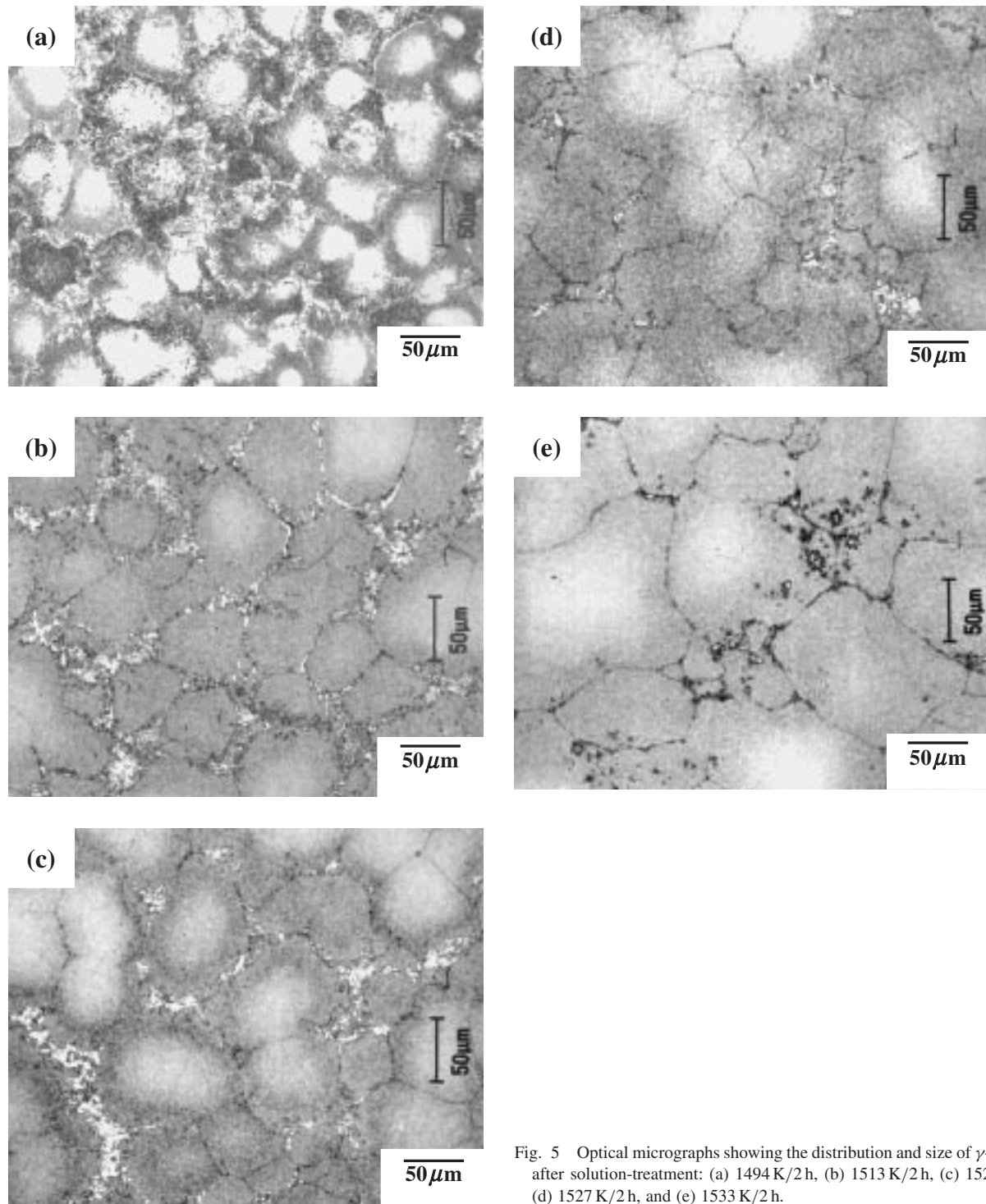


Fig. 5 Optical micrographs showing the distribution and size of  $\gamma$ - $\gamma'$  phase after solution-treatment: (a) 1494 K/2 h, (b) 1513 K/2 h, (c) 1522 K/2 h, (d) 1527 K/2 h, and (e) 1533 K/2 h.

about 10 K above the liquidus. The  $\gamma'$  particle size is about 0.3  $\mu\text{m}$  and the particles are spherical or cubic, as indicated in Fig. 4(a). The low pouring temperature causes the liquid metal in this study to be more viscous than that used in conventional casting, and pores can be formed in the as-cast structure. Therefore, castings produced by the Microcast-X process must also undergo Hot Isostatic Pressing (HIP) to eliminate all micropores.<sup>2)</sup> The high soaking temperature and the low cooling rate cause the  $\gamma'$  particles to be slightly larger (at about 0.5–1.0  $\mu\text{m}$ ) following HIPing, as presented in Fig.

4(b), but with almost unchanged shapes. After HIP cycles, the alloys were heat-treated to control the morphology of  $\gamma$ - $\gamma'$  eutectic phases,  $\gamma'$  particles and carbides to improve the mechanical properties of the alloy.

Figure 5 shows the morphology of the  $\gamma$ - $\gamma'$  eutectic phase after solution-treatment at various temperatures. The solution of eutectic  $\gamma$ - $\gamma'$  phase proceeded by increasing the multi-step solution-treatment temperature. However, multi-step 1533 K/2 h solution-treatment is inappropriate because of slight incipient melting, which occurred as depicted in Fig.



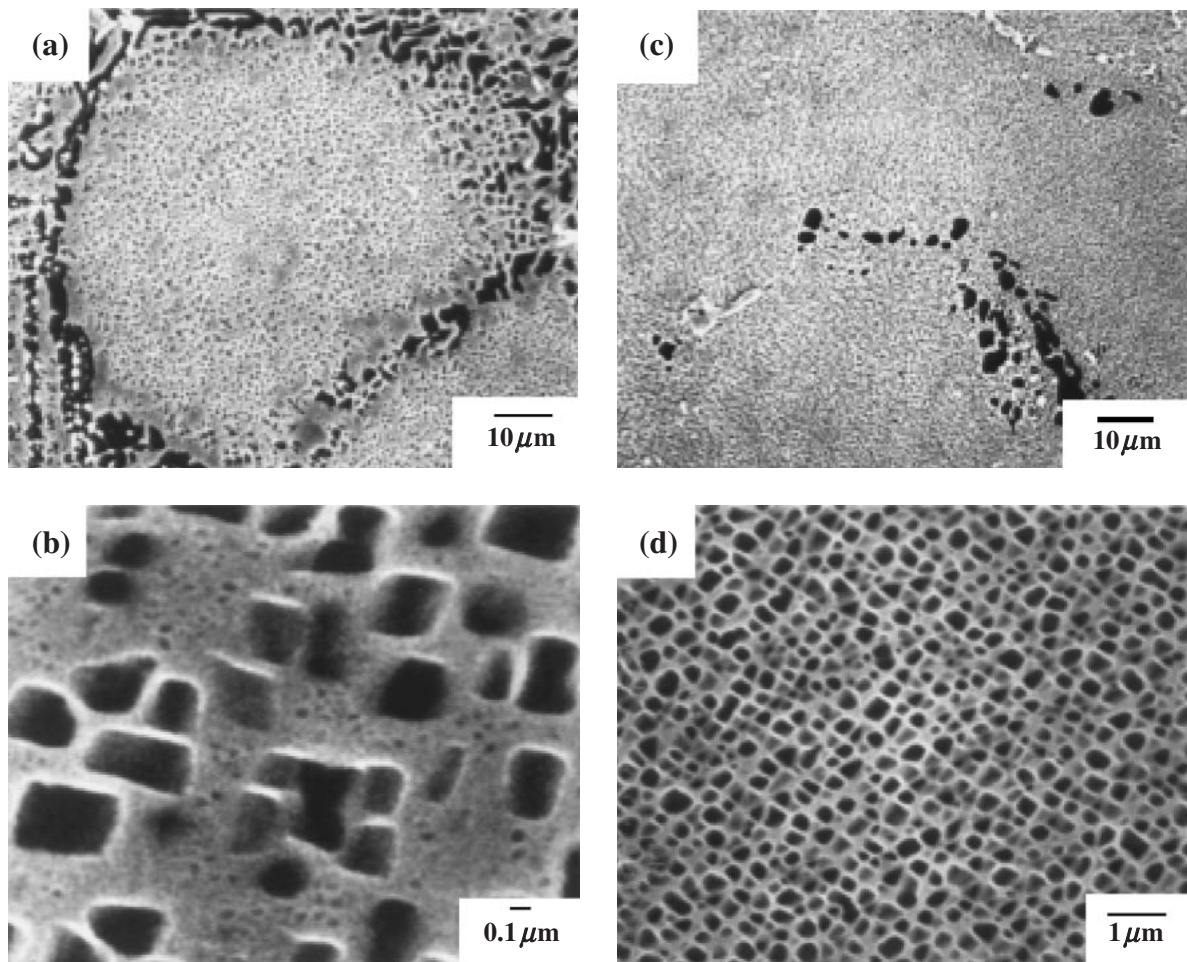


Fig. 6 SEM micrographs showing the distribution and size of  $\gamma'$  phase after multi-step 1494 K/2 h + 1353 K/4 h + 1144 K/20 h heat treatment observed at (a) grain boundary, and (b) matrix and after 1527 K/2 h + 1353 K/4 h + 1144 K/20 h heat treatment observed at (c) grain boundary, and (d) the center of grain.

5(e). Hence, the multi-step 1527 K/2 h solution-treatment is optimal. Furthermore, Figs. 5(a)–(d) show that solution-treatment at 1494 K–1527 K/2 h did not at all influence the grain size, which was about 60–70  $\mu\text{m}$  as small as the castings. However, Fig. 5(e) indicates that the grain size after the final step at a temperature of 1533 K/2 h greatly exceeded that of the as-cast superalloy.

Moreover, the SEM micrograph in Figs. 6(a) and (b) show that the fine-grain CM 247 LC superalloy having undergone 1494 K/2 h + 1353 K/4 h + 1144 K/20 h heat treatment, exhibits two  $\gamma'$  particle sizes; most particles are larger than 0.6  $\mu\text{m}$ , and a few are smaller than 0.05  $\mu\text{m}$ . In contrast, Figs. 6(c) and (d) reveal that the fine-grain CM 247 LC superalloy having undergone multi-step 1527 K/2 h + 1353 K/4 h + 1144 K/20 h heat treatment, exhibits uniformly distributed  $\gamma'$  particle sizes from 0.3 to 0.5  $\mu\text{m}$ .

The as-cast carbide is predominantly script-like. Figure 7 shows changes of the carbide morphology after solution-treatment at various temperatures. Increasing the temperature of multi-step solution-treatment alters the morphology of the carbides from script-like to globular and discrete. Moreover, SEM/EDS (Table 2) indicates that the MC carbides are predominantly (Ta,Ti)-rich carbides. However, solution-treatment transforms the carbides into more stable (Hf,Ta)-

rich carbides.

### 3.2 Tensile test

Figure 8 shows the tensile properties at 300 K of the alloys after solution-treatment at various temperatures. The yield strength increases from 915 MPa for test bars that have undergone solution-treatment at 1494 K/2 h to 993 MPa for test bars that have undergone multi-step 1527 K/2 h solution-treatment, with only a slight decline in both ultimate tensile strength and elongation, as shown in Figs. 8(b) and (c). However, after multi-step 1533 K/2 h solution-treatment, the ultimate tensile strength and ductility drop sharply. Moreover, the ultimate tensile strength and total elongation have peak values at 1513 K, whilst the yield strength peaks at 1527–1533 K.

### 3.3 Creep and rupture tests

Figure 9 plots the stress-rupture properties of the superalloy tested at 1255 K. When the test condition shifts from low stress (104 MPa) to high stress (345 MPa) at 1255 K, the alloy after multi-step 1527 K/2 h solution-treatment has a superior rupture life than the alloy after 1494 K/2 h solution-treatment.

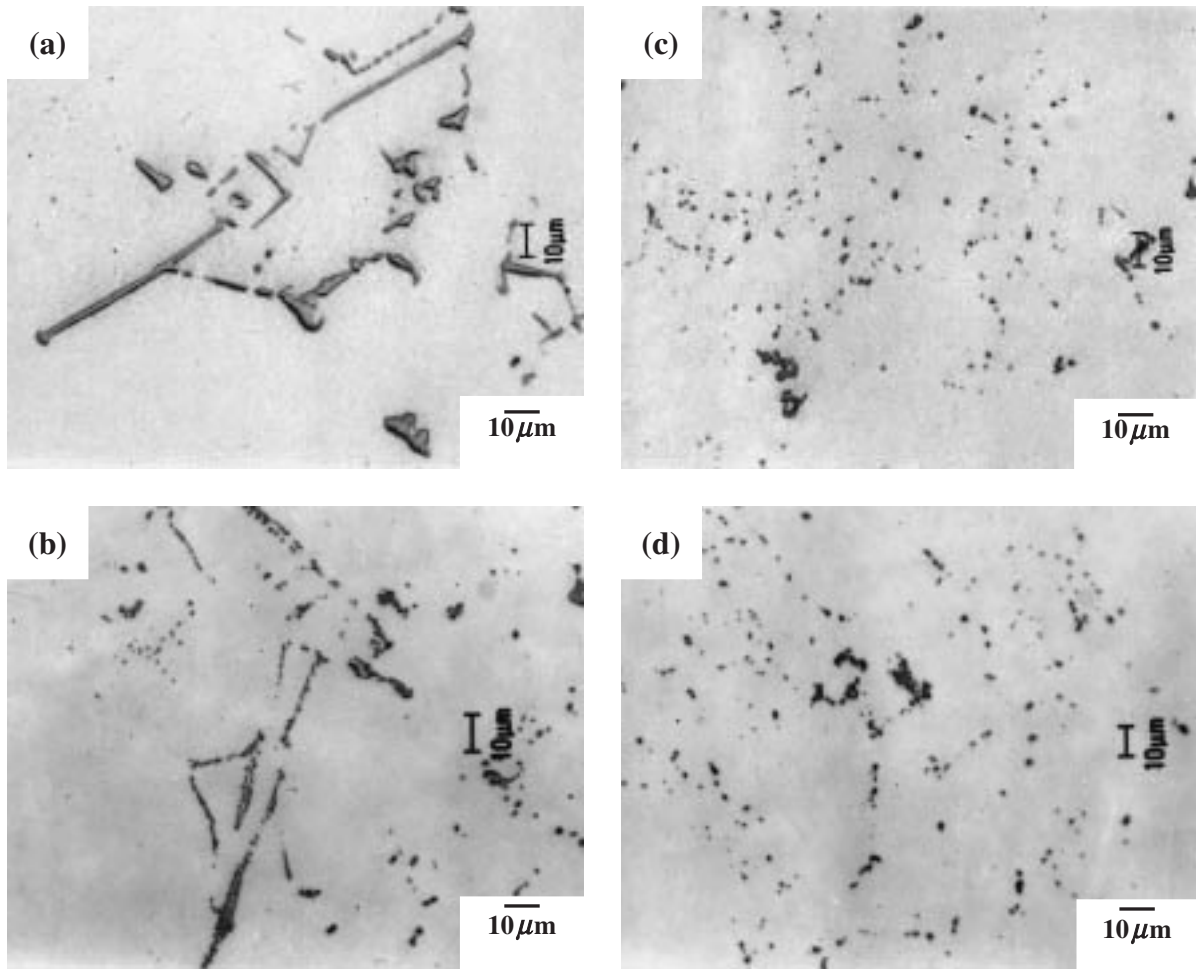


Fig. 7 Optical micrographs showing the morphology of carbide at various solution-treatment temperatures: (a) as-cast, (b) 1494 K/2 h, (c) 1527 K/2 h, and (d) 1533 K/2 h.

Table 2 The SEM-EDS analysis of carbide in fine-grain CM 247 LC superalloy.

Condition	GB carbide	Matrix carbide
Casting	(Ta, Ti)-rich	(Ta, Ti, Hf)-rich
HIPing + 1494 K/2 h Solution-Treatment	(Ta, Hf)-rich	(Hf, Ta)-rich
HIPing + Multi-step 1527 K/2 h Solution-Treatment	(Ta, Hf)-rich	(Hf, Ta)-rich

## 4. Discussion

### 4.1 Volume fraction and size of $\gamma'$ particles

Nickel-based superalloys may be strengthened by  $\gamma'$  precipitation in a fcc  $\gamma$  matrix. Many factors affect strengthening by  $\gamma'$ , including volume fraction and size of  $\gamma'$  particle.

All the dislocation cutting models in previous reports agree that when particles grow beyond a critical size,<sup>10,11</sup> bypass may occur by bowing, climbing or other processes. The Orowan bowing model<sup>12</sup> is generally considered to be most applicable to austenitic superalloys. The increment in flow stress at low temperatures due to bowing, is evaluated by considering the radius of curvature  $\rho$  to which a flexible dislocation can be bent by an applied stress  $\tau$ ,

$$\tau b = T/\rho$$

The minimum value of  $\rho$  is half of the inter-particle spacing  $L$  and corresponds to  $\theta = 1/2\pi$ , where  $\theta$  is the angle between the dislocation line and its Burgers vector. The line tension  $T$  is given approximately by  $1/2Gb^2$  (where  $b$  is the magnitude of the Burgers vector of the piled-up dislocations), but a more exact formulation<sup>13</sup> is

$$T = (Gb^2/4\pi)\phi' \ln(L/2b),$$

where  $\phi' = 1/2[1 + 1/(1 - \nu)]$ , and  $\nu$  and  $G$  are the Poisson's ratio and shear modulus of the matrix, respectively. Additionally,  $L$  is assumed to be the edge-to-edge spacing of the particles. Therefore, the following expression is given for the increment in flow stress  $\Delta\tau$ :

$$\Delta\tau = (Gb/2\pi L)\phi' \ln(L/2b)$$

Increasing the volume fraction  $f$  for a given particle size to reduce  $L$ , increases the strength. The multi-step dissolving process is more effective at 1527 K/2 h than at low temperature, and results in improved yield strength, due to the increased volume fraction of finely re-precipitated  $\gamma'$  phase, or decreased interparticle spacing ( $L$ ).

The creep deformation map of a CM 247 LC-related superalloy<sup>14</sup> shows that the creep mechanism under the

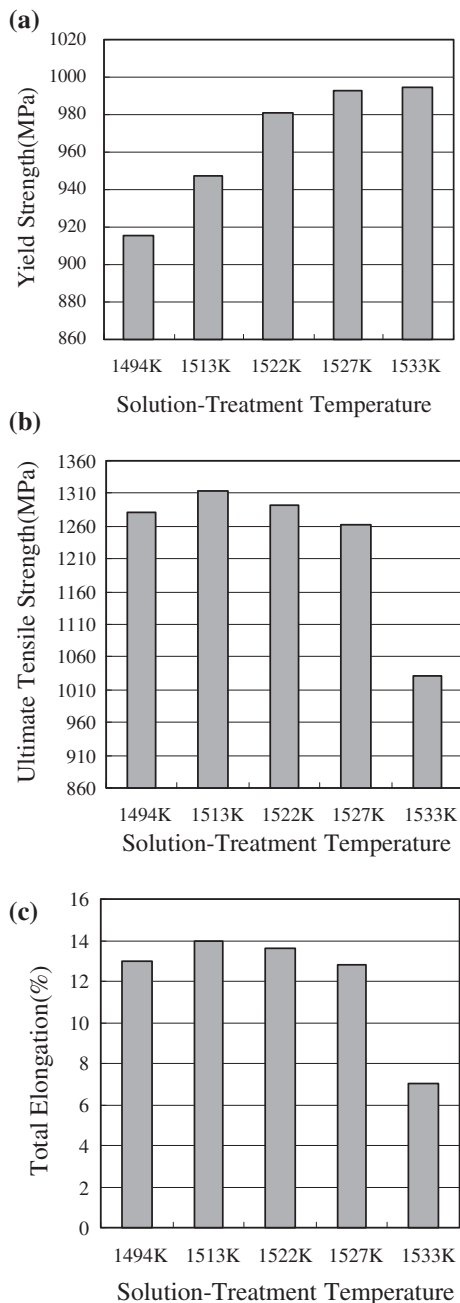


Fig. 8 The variation of the (a) yield strength, (b) ultimate tensile strength and (c) total elongation as a function of solution-treatment temperature.

conditions 104 MPa–345 MPa/1255 K involves dislocation climb; that is, the creep behavior is dominated by the interaction between dislocations and obstacles such as  $\gamma'$  particles or carbides. Sims *et al.*<sup>15)</sup> stated that the  $\gamma'$  particles in the superalloy with size from 0.25 to 0.50  $\mu\text{m}$  help to inhibit dislocation climb at 1255 K.

The  $\gamma'$  phase was observed as either a spherical or a cubic precipitate; its shape was found to be related to the matrix-lattice mismatch. Hagel and Beattie<sup>16)</sup> observed that precipitates were spheres at a 0–0.2% lattice mismatch, cubes at a mismatch of 0.5%–1.0%, and plates at a mismatch higher than 1.25%.

The partial dissolution of the coarse  $\gamma$ – $\gamma'$  eutectic phase and the coarse  $\gamma'$  phase at 1494 K/2 h leads to the over-aging

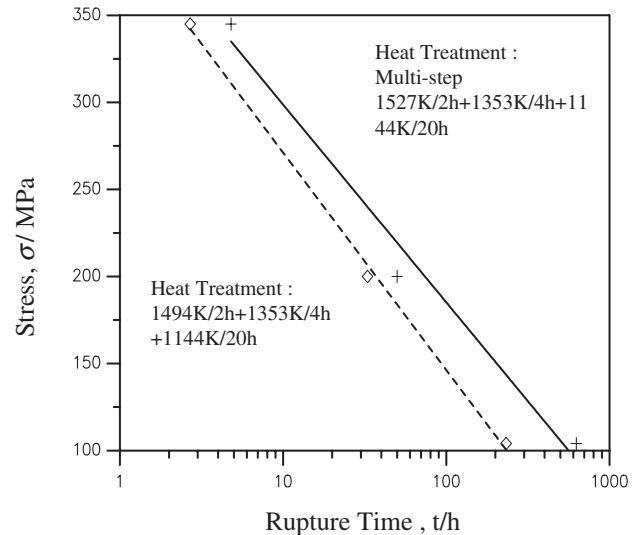


Fig. 9 Stress-to-rupture life at 1255 K for fine-grain CM247 LC superalloy completely multi-step 1527 K/2 h solution-treated and double aged compared with those partially 1494 K/2 h solution-treated and double aged.

and growth of  $\gamma'$  particles after double aging heat-treatment at 1353 K/4 h + 1144 K/20 h. The growth of  $\gamma'$  particles and the reduced number of  $\gamma'$  particles may increase the interparticle spacing. Therefore, when  $\gamma'$  particles are exposed at 1255 K, the coarse  $\gamma'$  particles ripen (become larger) at a significant rate and the interparticle spacing increases, facilitating dislocation bypassing.

Conversely, the optimal dissolution of the coarse  $\gamma$ – $\gamma'$  eutectic phase and the coarse  $\gamma'$  phase at 1527 K/2 h causes the re-precipitation of a high volume fraction of  $\gamma'$  particle size of uniform size with a small interparticle spacing, inhibiting the bowing and climbing of dislocations. Therefore, the loss of creep resistance during  $\gamma'$  ripening depends strongly on the volume fraction of the re-precipitated  $\gamma'$  phase, because the fine-grained CM247LC superalloy with a low volume fraction of re-precipitated  $\gamma'$  phase weakens more quickly than that with high volume fraction of re-precipitated  $\gamma'$  phase. Accordingly, increasing the volume fraction of the moderate  $\gamma'$  phase promotes the creep performance at 1255 K in a fine-grain CM 247 LC superalloy.

#### 4.2 Morphology of carbide

Usually, conventionally cast nickel-based superalloys are strengthened mainly by carbide precipitation at the grain boundary and the  $\gamma'$  phase in the matrix. Hence, the morphology and distribution of carbide are crucial in determining the creep behavior and ductility of superalloys at high temperature. In the late 1970s, alloy designers added Hf into Ni-based superalloys to produce the  $\gamma$ – $\gamma'$  eutectic phase and increase the toughness of GB.<sup>17–20)</sup> However, nickel-based cast superalloy remained brittle at elevated temperatures.<sup>20)</sup> Fractographic observations revealed that cracks are preferentially initiated at the MC carbide/matrix interface in Mar-M247 superalloys at elevated temperatures.<sup>21)</sup> Kaufman obtained the same results<sup>22)</sup> and proved that script-like MC carbides are extremely brittle and may act as crack initiation sites or crack propagation paths. Baldan<sup>23)</sup>

also noted that the size of the carbide particles dominates the creep rupture, and that fine dispersion increases creep ductility.

In this study, increasing the temperature of the solution from 1494 K/2 h to 1533 K/2 h markedly refines carbides in the matrix and at the grain boundary, and makes them spherical. Blocky carbide particles at grain boundaries may act as dispersed obstacles that retard sliding of the grain-boundary and form barriers to crack propagation. Therefore, for the fine-grain CM 247 LC superalloy, increasing the dissolution temperature (1527 K/2 h) can promote the creep life (1255 K) and the yield strength at high temperature. Additionally, the ductility maintains at 12–13% for total elongation even though the yield strength is highly improved by increasing the volume fraction of the uniform  $\gamma'$  phase. The fine carbide particles at the grain boundaries may reduce the mobility of the grain boundaries and absorb the energy of deformation, hence both the ultimate tensile strength and the total elongation initially increase with the dissolution temperature. Moreover, Sims<sup>24)</sup> indicated that coarse  $\gamma'$  and  $\gamma$ - $\gamma'$  depletion near the grain boundary in high strength nickel alloys may also form a ductile zone, preventing the initiation of grain-boundary fracture through enhanced the local ductility. However, increasing the dissolution temperature from 1494 K/2 h to 1533 K/2 h reduces the size of the ductile zone (Fig. 5), which has a low effective elastic modulus, leading to stress concentrations at the grain boundaries and reducing the absorption of energy of deformation. Hence, both the ultimate tensile strength and the total elongation decline as the dissolution temperature rises over 1513 K/2 h. Therefore, the ultimate tensile strength and elongation are maximal at 1513 K.

## 5. Conclusion

- (1) Multi-step 1527 K/2 h solution-treatment increased the volume fraction of relatively fine  $\gamma'$  particles and refined the carbides in fine-grain CM 247 LC superalloy.
- (2) The yield strength at 300 K increased after multi-step 1527 K/2 h solution-treatment, whilst the ductility was maintained as high as 12–13% of the total elongation.
- (3) The creep rate and rupture life were improved after multi-step 1527 K/2 h solution-treatment. Improvements of the mechanical properties are attributed to

the microstructure, and particularly the morphology of  $\gamma'$  particles and carbides.

## Acknowledgements

The authors would like to thank the National Science Council of the Republic of China for financially supporting this research under Contract No. NSC 91-2623-7-002-008.

## REFERENCES

- 1) M. Kaufman: *Proc. Superalloys 1984*, M. Gell, ed., (AIME, Warrendale, PA, 1984) pp. 43–52.
- 2) M. Wouds and H. Benson: *Proc. Superalloys 1984*, M. Gell, ed., (AIME, Warrendale, PA, 1984) pp. 3–14.
- 3) B. A. Ewing and K. A. Green: *Proc. Superalloys 1984*, M. Gell, ed., (AIME, Warrendale, PA, 1984) pp. 33–42.
- 4) C. T. Sims, N. S. Stoloff and W. C. Hagel: *Superalloy II*, (John Wiley & Sons, New York, 1987) pp. 425–426.
- 5) G. K. Bouse and M. R. Behrendt: *Superalloy 718*, E. A. Loria, ed., (TMS, Warrendale, PA, 1989) pp. 319–328.
- 6) K. Harris and R. E. Schwer: TMS-AIME Fall Meeting, St. Louis, MO, (1978) pp. 1–11.
- 7) K. Harris and R. E. Schwer: AVS 6th Int. Vac. Met. Conf., (San Diego, CA, 1979) pp. 7–8.
- 8) K. Harris, G. L. Erickson and R. E. Schwer: 5th Int. Symposium on Superalloys, (Champion, PA, 1984) pp. 221–230.
- 9) H. E. Huang and C. H. Koo: *Chinese Journal of Materials Science and Engineering* **32** (2000) 170–176.
- 10) R. K. Ham: *Ordered Alloys; Structural Applications and Physical Metallurgy*, (Claitors, Baton Rouge, LA, 1970) pp. 365–373.
- 11) H. Gleiter and E. Hombogen: *Mater. Sci. Eng.* **2** (1968) 285–302.
- 12) E. Orowan: *Symposium on Internal Stresses in Metals*, (Institute of Metals, London, 1948) pp. 451–453.
- 13) A. Kelly and R. B. Nicholson: *Prog. Mater. Sci.* **10** (1963) 151–191.
- 14) C. T. Sims, N. S. Stoloff and W. C. Hagel: *Superalloy II*, (John Wiley & Sons, New York, 1987) pp. 39–40.
- 15) C. T. Sims, N. S. Stoloff and W. C. Hagel: *Superalloy II*, (John Wiley & Sons, New York, 1987) pp. 208–210.
- 16) W. C. Hagel and H. J. Beattie: *Iron and Steel Inst. Spec.* (1964) pp. 98–107.
- 17) J. E. Doherty, B. H. Kear and A. F. Giamei: *J. Met.* **23** (1971) 59–62.
- 18) D. N. Dahi and C. P. Sullivan: *J. Met.* **23** (1971) 38–40.
- 19) P. S. Kotval, J. D. Venables and R. W. Calder: *Metall. Trans.* **3** (1972) 453–458.
- 20) H. Y. Bor, C. G. Chao and C. Y. Ma: *Scr. Mater.* **38** (1998) 329–335.
- 21) H. Y. Bor, C. G. Chao and C. Y. Ma: *Metall. Mater. Trans. A* **30** (1999) 551–561.
- 22) M. Kaufman: *Proc. Superalloys 1984*, M. Gell, ed., (AIME, Warrendale, PA, 1984) pp. 43–52.
- 23) A. Baldan: *Z. Metallkd.* **83** (1992) 750–757.
- 24) C. T. Sims: *J. Met.*, **18** (1966) 1119–1130.